Flamelet-Based Modeling of H2/Air Auto-Ignition with Thermal Inhomogeneities

David J. Cook[1]*, Jacqueline H. Chen[2], Evatt R. Hawkes[2], Ramanan Sankaran[2], and Heinz Pitsch[1]

[1] Department of Mechanical Engineering, Stanford University, Stanford, California 94305

[2] Sandia National Laboratories, Livermore, California 94551

Paper # 05F-68

Presented at the Western States Meeting of the Combustion Institute, Oct 2005, Stanford, CA

ABSTRACT

Homogeneous-Charge Compression Ignition (HCCI) engines have been shown to have higher thermal efficiencies and lower NO_x and soot emissions than Spark Ignition engines. However, HCCI engines experience very large heat release rates which can lead to the occurrence of damaging engine knock. One method of reducing the maximum heat release rate is to introduce thermal inhomogeneities, thereby spreading the heat release over several crank angle degrees. Direct Numerical Simulations (DNS) with complex H_2/Air chemistry by Hawkes et al. (2005) showed that both ignition fronts and deflagration-like fronts are present in systems with such inhomogeneities. Here, an enthalpy-based flamelet model is presented and applied to the four cases of varying initial temperature variance presented in Hawkes et al. (2005). This model uses a mean scalar dissipation rate to model the mixing between regions of higher and lower enthalpies. The predicted heat release rates agree well with the heat release rates of the four DNS cases. Although this model does not treat ignition fronts and deflagration-like fronts differently, here it is shown to be capable of capturing the combustion characteristics for both the case in which combustion occurs primarily in the form of spontaneous ignition fronts and for the case dominated by deflagration-type burning. The flamelet-based model shows considerably improved agreement with the DNS results over the popular multi-zone model, particularly, where both deflagrative and spontaneous ignition are occurring, that is, where diffusion is important.

INTRODUCTION

Homogeneous-Charge Compression Ignition (HCCI) engines have recently been the subject of much research effort for both their low NO_x(oxides of nitrogen) and soot emissions, and higher thermal efficiency compared to Spark Ignition (SI)

*Email: david.cook@stanford.edu

engines. While significant progress has been made, these engines continue to suffer from high carbon monoxide (CO) and unburnt hydrocarbon (UHC) emissions. Additionally, HCCI engines experience high heat release rates, which sometimes can lead to engine damaging knock-like phenomena. Both the CO and UHC emissions and the heat release rates are strongly related to the level of temperature and mixture composition inhomogeneities in the cylinder gases.

While HCCI refers to a type of combustion which typically has a homogeneous charge in terms of mixture composition, the charge experiences large stratification in the enthalpy field due to wall heat loss or heating because of hot valves combined with incomplete turbulent mixing between the bulk gases and gases in near wall regions. This stratification typically causes regions in the center of the cylinder to ignite first, followed later by regions closer to the cylinder walls. This stratification can lead to the occurrence of both volumetric and front-like combustion modes. HCCI engines also have stratification of mixture composition due to incomplete mixing of the Exhaust Gas Recirculation (EGR) and the fresh charge, or due to late phased Direct Injection (DI). Here, only the effects of thermal inhomogeneities will be considered. These effects on CO and UHC emissions and on heat release rates will be briefly discussed below.

The relatively high CO emissions in HCCI engines are a consequence of the strategy used to achieve the main goal of reducing NO_x. Experimentally, it has been found that CO emissions originate in regions where the gas temperature does not exceed 1500 K [3]. Yet, in order to limit NO_x emissions, HCCI engines are run in a way that achieves low peak temperatures. This is generally accomplished by running the engines very lean or, more commonly, highly diluted with significant internal or external EGR. Such operating strategies can result in a maximum burnt gas temperature below 1850 K, and therefore lead to low NO_x emissions. Having a maximum burnt gas temperature below 1850 K in the cylinder implies that regions strongly affected by wall heat loss conditions will be favorable for producing higher CO emissions.

Unburnt hydrocarbon emissions come from regions in the cylinder where auto-ignition does not occur. These regions are typically either extremely dilute, as in the case of a partially stratified charge from direct injection, or are strongly affected by wall heat loss, or both. Another major cause of UHC emissions is cycles in which misfire occurs. However, as control of ignition timing in HCCI engines improves, this cause of UHC emissions will likely become less significant.

The presence of thermal inhomogeneities tends to decrease the maximum heat release rates by spreading it over several crank angle degrees. One possible strategy to suppress the occurrence of engine knock is to introduce inhomogeneities of temperature or mixture fraction in order to produce the desired heat release rate [2]. A charge with non-negligible levels of thermal inhomogeneities will have some hot and some cold regions. Gas in the hot regions will tend to ignite first, followed by regions that are a little cooler, until finally, the gas in the cold regions ignites. The larger the level of inhomogeneity, the lower the maximum heat transfer rates will be.

Thus, thermal inhomogeneities affect the combustion emissions and heat release rates in HCCI engines. As experimental data suggests that cylinder flow and turbulence play an important role in HCCI combustion [1], a better understanding of its interaction with chemical kinetics could be used to reduce CO and UHC emissions and control the heat release rates in HCCI engines. These affects have been modeled using multiple zones, where ignition of gas with a smaller enthalpy defect (i.e. gases less affected by wall heat loss) affects gases with higher levels of enthalpy defect only through the increased pressure associated with the volumetric expansion of the ignited gases [4, 5, 6]. Additionally, fully coupled CFD and chemistry studies have been done, in which the chemical source terms have been evaluated using mean values, and a low-order correction for the effects of turbulence have been used in the combustion process [7]. In the present study, the effect of thermal inhomogeneities on combustion is modeled using a flamelet-based approach proposed by Cook et al. [8]. In this model the flamelet equations are solved in a normalized enthalpy space. Transport across this enthalpy space physically represents interaction between gases of higher and lower levels of enthalpy defect. The model is validated using DNS data of constant volume auto-ignition of H_2/air with thermal inhomogeneities conducted by Hawkes et al. [9]. Results are compared with an idealized multizone model.

ENTHALPY-BASED FLAMELET MODELING

In this section, a derivation of the enthalpy-based flamelet equations will be given. The general equations for species mass-fraction transport and total enthalpy transport are as follows

$$\rho\frac{\partial Y_i}{\partial t}+\rho v_j\frac{\partial Y_i}{\partial x_j} = \frac{\partial}{\partial x_j}\left(\rho D\frac{\partial Y_i}{\partial x_j}\right)+\rho\dot{\omega}_i\,, \tag{1}$$

$$\rho\frac{\partial H}{\partial t}+\rho v_j\frac{\partial H}{\partial x_j} = \frac{\partial}{\partial x_j}\left(\rho D\frac{\partial H}{\partial x_j}\right)+\left(\frac{\partial p}{\partial t}-\dot{q}_{\Delta\mathrm{h}}\right), \tag{2}$$

where Y_i is mass fraction of species i, H is total enthalpy, ρ is density, D is molecular diffusivity assumed equal for all species, $\dot{\omega}_i$ is the chemical source term for species i, p is pressure, $\dot{q}_{\Delta\mathrm{h}}$ accounts for volumetric heat loss such as radiation, and v_j is the velocity in the x_j-direction. The (x_1, x_2, x_3)-coordinate system can be transformed into a system which locally aligns with the enthalpy gradients. In the following analysis of this transformation, the x_1-coordinate is assumed to be normal, and the x_2 and x_3-coordinates are assumed to be tangential to an iso-enthalpy surface. This transformation is made such that

$$(t, x_1, x_2, x_3) \rightarrow (\tau, H, H_2, H_3), \tag{3}$$

where enthalpy is introduced as a new independent coordinate. This implies that the new independent coordinate, H, is attached to an iso-surface of enthalpy and that the new coordinates H_2 and H_3 lie within this surface. Hence this transformation in space and in time coordinates is defined as

$$\begin{aligned}\frac{\partial}{\partial t} &= \frac{\partial}{\partial \tau}+\frac{\partial H}{\partial t}\frac{\partial}{\partial H}\,,\\ \nabla &= \nabla_H\frac{\partial}{\partial H}+\nabla_{H_\perp},\ \text{with}\ \nabla_{H_\perp}=\begin{pmatrix}0\\ \partial/\partial H_2\\ \partial/\partial H_3\end{pmatrix}.\end{aligned} \tag{4}$$

If the gradients in the H-coordinate are assumed to be large compared to gradients in the H_2 and H_3 directions, then an asymptotic analysis similar to the one used by Peters (2000) [10] for the mixture fraction formulation of the flamelet equations can be applied. After such analysis, it can be shown that terms in the flamelet equations which include gradients in the H_2 and H_3 directions are small compared to other terms and therefore can be neglected.

The fundamental assumption mentioned above, namely that the gradients in the H-direction are large compared to gradients in the H_2 and H_3 directions, requires further discussion. The following arguments are presented for systems with inhomogeneities in enthalpy, but with initially perfectly homogeneous mixture composition.

Chemical reactions in combustion systems are governed by Arrhenius rate expressions in which the reaction rates have an exponential dependence on temperature. The total enthalpy before ignition, defined to include the heat of formation of the species in the mixture, is directly related to temperature through the specific heat. This implies that before ignition, the reaction rates also have exponential dependence on the enthalpy. Because of this, chemical reactions, especially during the early stages of the ignition process, will only occur around a thin layer of the surface of the most favorable enthalpy. Away from this surface, the reaction rates become exponentially smaller. Therefore, variations in species concentration and temperature in the H-coordinate prior to ignition will be large compared to variations in the H_2 and H_3 directions. Prior to ignition, $\nabla_{H_\perp}$ is hence small compared to $\nabla_H\frac{\partial}{\partial H}$.

After gases at higher enthalpies have ignited, large spatial gradients in species concentration and temperature will exist between the unburnt and the ignited gases. Chemistry will then tend to be most active in thin layers between unburnt and already ignited mixtures where thermal and species transport is large due to large local gradients. Transport across the thin layers of most active chemistry in this case will mainly align with the enthalpy gradients and diffusion normal to the enthalpy gradients will be smaller. This process essentially describes a premixed flame front moving into gases of lower temperature. The above assumption is then valid as long as the width of this thin layer is smaller than the smallest length scale of the turbulence.

This above discussion is particularly valid in the case of large enthalpy gradients. In the case of small enthalpy gradients, diffusion is slow compared to chemistry. Therefore, combustion during ignition can be approximated as a series of homogeneous reactors. Hawkes et al. [9] conducted a DNS of two-dimensional turbulence with detailed hydrogen/air

chemistry where small fluctuations in unburnt temperature were modeled accurately using a multizone model in which diffusive transport effects were not included. For the case of small enthalpy gradients, they showed that the chemical source term was the dominant term and that effects of diffusive transport were comparatively negligible. Therefore, for the case of small gradients, diffusion is negligible and exclusion of the $\nabla_{H_\perp}$ term in the coordinate transformation will result in only negligible errors. Hence, for both cases of large and small gradients the $\nabla_{H_\perp}$ term is small compared to gradients along constant contours of enthalpy, and therefore this term is neglected in this study.

Applying Eq.(4) to Eq.(1) and neglecting the $\nabla_{H_\perp}$-terms results in

$$\rho\frac{\partial Y_i}{\partial \tau} = - \frac{\partial Y_i}{\partial H}\left(\rho\frac{\partial H}{\partial t} + \rho v_j \frac{\partial H}{\partial x_j}\right) + \frac{\partial Y_i}{\partial H}\left(\frac{\partial}{\partial x_j}\left(\rho D \frac{\partial H}{\partial x_j}\right)\right) + \rho D \frac{\partial H}{\partial x_j}\frac{\partial H}{\partial x_j}\frac{\partial^2 Y_i}{\partial H^2} + \rho\dot{\omega}_i \tag{5}$$

Introducing a scalar dissipation rate in enthalpy-space,

$$\chi_{_H} \equiv 2D\frac{\partial H}{\partial x_j}\frac{\partial H}{\partial x_j}, \tag{6}$$

substituting Eq.(2) into Eq.(5), and canceling similar terms produces,

$$\rho\frac{\partial Y_i}{\partial \tau} + \left(\frac{\partial p}{\partial t} - \dot{q}_{\Delta \mathrm{h}}\right)\frac{\partial Y_i}{\partial H} = \frac{\rho\chi_{_H}}{2}\frac{\partial^2 Y_i}{\partial H^2} + \rho\dot{\omega}_i\,. \tag{7}$$

The second term on the left hand side represents a convection term in enthalpy space. This term is not present in the mixture fraction formulation of the flamelet equations because mixture fraction is a conserved scalar, while enthalpy is not. The temperature equation can similarly be expressed in enthalpy space.

In order to simplify the numeric solution of the these equations, we normalize the enthalpy field and define a new coordinate ξ as

$$\xi = \frac{H - \Theta_{\min}(\tau)}{\Theta_{\max}(\tau) - \Theta_{\min}(\tau)} = \frac{H - \Theta_{\min}(\tau)}{\Delta\Theta(\tau)}\,. \tag{8}$$

$\Theta_{\min}(\tau)$ and $\Theta_{\max}(\tau)$ represent the minimum and maximum possible enthalpies in the system, as defined in the appendix (Eqs. 17 & 18), so that $0 \leq \xi \leq 1$.

Applying transformation derivatives, as defined in the appendix, and defining a normalized scalar dissipation rate ($\chi_\xi = \chi_{_H}/(\Delta\Theta)^2$), we finally obtain the following form of the flamelet equations

$$\rho\frac{\partial Y_i}{\partial \tau^\star} = - \rho v_\xi \frac{\partial Y_i}{\partial \xi} + \frac{\rho\chi_\xi}{2}\frac{\partial^2 Y_i}{\partial \xi^2} + \rho\dot{\omega}_i \tag{9}$$

$$\rho\frac{\partial T}{\partial \tau^\star} = - \rho v_\xi \frac{\partial T}{\partial \xi} + \frac{\rho\chi_\xi}{2}\frac{\partial^2 T}{\partial \xi^2} + \frac{\rho\chi_\xi}{2C_p}\frac{\partial T}{\partial \xi}\left(\frac{\partial C_p}{\partial \xi} + \sum_i^{\mathrm{N}} c_{p,i}\frac{\partial Y_i}{\partial \xi}\right) - \frac{\rho}{C_p}\sum_i^{\mathrm{N}} h_i\dot{\omega}_i + \frac{1}{C_p}\left(\frac{\partial p}{\partial t} - \dot{q}_{\Delta h}\right). \tag{10}$$

Here C_p represents the specific heat of the mixture and v_ξ is the convective velocity in ξ-space as defined in the appendix by Eq.(30).

COUPLING FLAMELET CODE TO DNS DATA

A fully-implicit one-dimensional finite difference code was used to solve the combustion model, Eqs.(9) & (10). An equidistant grid of 101 points in ξ-space was used. From Eq.(8), we see that $\Theta_{\max}(\tau)$ and $\Theta_{\min}(\tau)$ are a function of time. These values were taken from the maximum and minimum total enthalpies found in the DNS at a given time. Additionally, the enthalpy dissipation rate, χ_H, as defined by Eq.(6), appears as a parameter in the flamelet equations. For this study it was taken to be the mean enthalpy dissipation rate conditioned on enthalpy from the DNS. Cubic splines were used to fit between DNS data outputs to make χ_H a function of time and normalized enthalpy. Furthermore, in

order to calculate the pressure, a Probability Density Function (PDF) of enthalpy is needed. This was also taken from the DNS data. Average species mass fractions and temperature were calculated by,

$$\widehat{Y_i} = \int_0^1 Y_i(\xi)P(\xi)d\xi \tag{11}$$

$$\widehat{T} = \int_0^1 T(\xi)P(\xi)d\xi\,, \tag{12}$$

where $P(\xi)$ is the PDF of normalized enthalpy taken from the DNS and $\widehat{\ }$ indicates a mean quantity for the system. An average molecular weight was then calculated using the relation

$$\widehat{W} = \left[\sum_i^N \frac{\widehat{Y_i}}{W_i}\right]^{-1}. \tag{13}$$

The average pressure was calculated from the mean quantities using

$$\widehat{p} = \frac{\widehat{\rho} R_u \widehat{T}}{\widehat{W}}\,, \tag{14}$$

where R_u is the universal gas constant. The time rate of change in average pressure was calculated using a second order upwinding Adams-Bashforth method. With these quantities, the flamelet code and DNS data are completely coupled and the flamelet equations are closed. Each of the five cases discussed below was calculated using this flamelet method with the same initial conditions and chemical mechanism as the DNS.

DIRECT NUMERICAL SIMULATION

To validate this modeling approach, DNS results of the auto-ignition of a lean hydrogen-air mixture in a closed volume in the presence of an inhomogeneous temperature field by Hawkes et al. [9] are used. The initial conditions include a uniform mixture composition field with equivalence ratio of 0.1, and initial pressure of 41 atm and a mean initial temperature of 1070 K. Further details of the DNS code, the initialization, and computational grid can be found in Ref. [9]. The DNS used a detailed H_2/air chemical mechanism by Mueller et al. [11] with 9 species and 42 reactions. The first four cases are identical, except that each had a different level of thermal stratification. The root-mean-square values of the initial temperature fluctuations, T', were 3.75 K, 7.5 K, 15 K and 30 K for the four cases respectively. A fifth case was done with a T' of 15K and a unity Lewis number. The only difference between case 3 and case 5 is that case 3 accounts for the effects of differential diffusion, while case 5 neglects these. A summary of these cases is given in Table 1.

CASE	T'	Differential Diffusion
1	3.75 K	Yes
2	7.5 K	Yes
3	15 K	Yes
4	30 K	Yes
5	15 K	No

Table 1: Summary of conditions for the 5 DNS cases.

RESULTS

First the results of the first four cases will be discussed. Figure 1 shows results for these cases from left to right. The top plots in Fig. 1 are the pressure for both DNS and flamelet model as a function of time normalized by the homogeneous

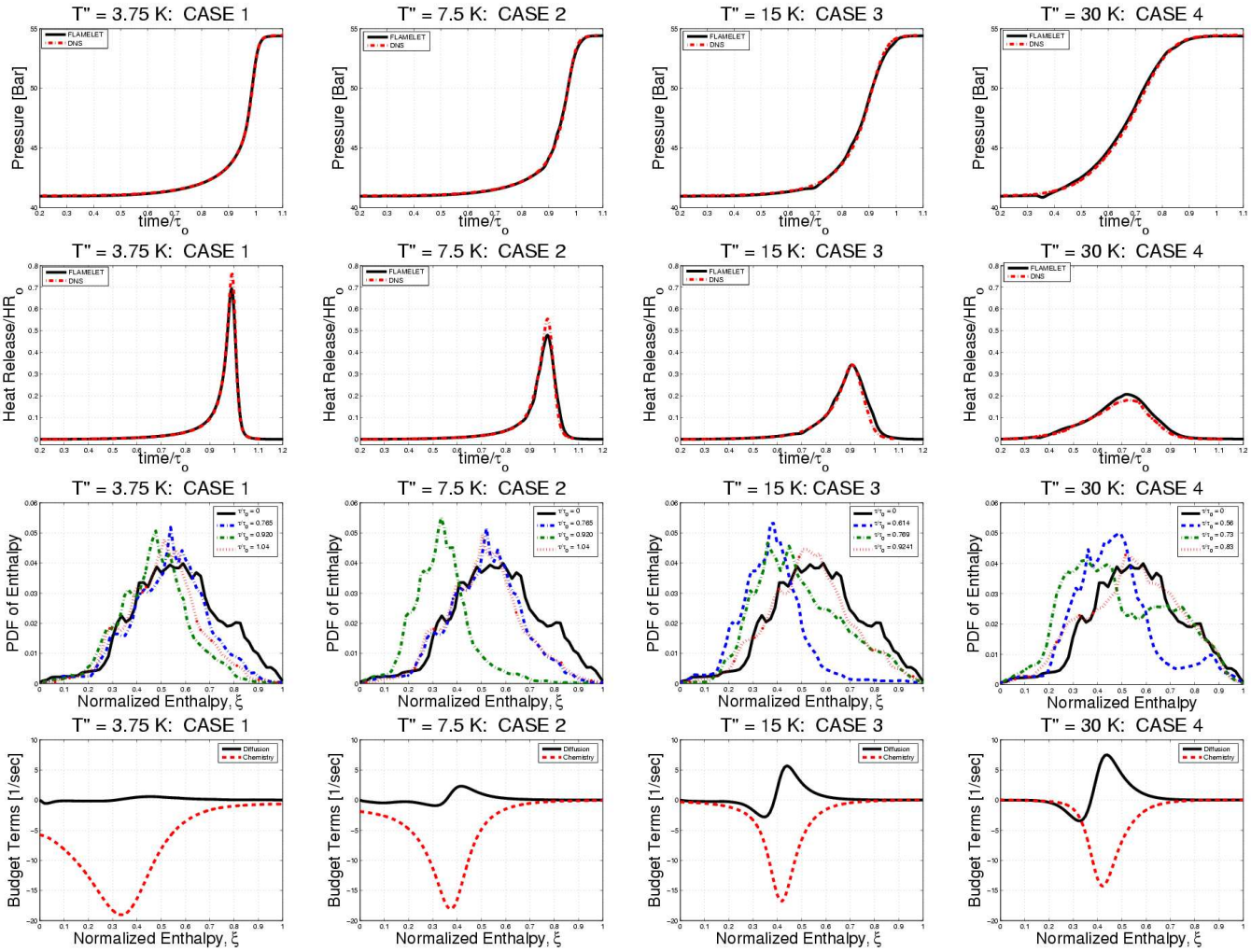

Figure 1: Heat release and pressure verses time for cases 1, 2, 3, and 4 both for DNS and flamelet model and budget terms for species mass fraction flamelet equation from simulation.

ignition delay time (2.9 ms). The DNS and flamelet model pressure curves are in good agreement for these four cases. The second row from the top in Fig. 1 is the heat release rate normalized by the maximum heat release rate of the homogeneous constant volume combustion case, and is plotted as a function of normalized time. The DNS and modeled heat release rates are also in very good agreement for these four cases. However, the flamelet model slightly underpredicts the maximum heat release rate for case 2 and over predicts the heat release rate for case 4. The third row from the top of Fig. 1 is the PDF of enthalpy plotted at various times for the four cases. For all but case 1, a high skewness of the PDF toward lower enthalpies is observed. Two primary influences lead to the distortion of the PDF away from its original shape. The PDF shifts toward lower normalized enthalpies during heat release because the regions which have already ignited have a lower density and therefore the pressure term in Eq.(10) increases their enthalpies faster than regions which have not ignited. A second influence leading to skewness is differential diffusion. Since hydrogen has a Lewis number significantly smaller than unity, it diffuses faster than most other species. Once ignition begins at high enthalpies, hydrogen diffuses from unburnt low enthalpy regions toward large enthalpy regions, effectively increasing the enthalpy at higher enthalpies and decreasing the enthalpy at lower enthalpies. Finally, the bottom row in Fig. 1 shows the magnitude of the diffusion term and chemical source term in the hydrogen mass fraction equation, Eq.(9), which are

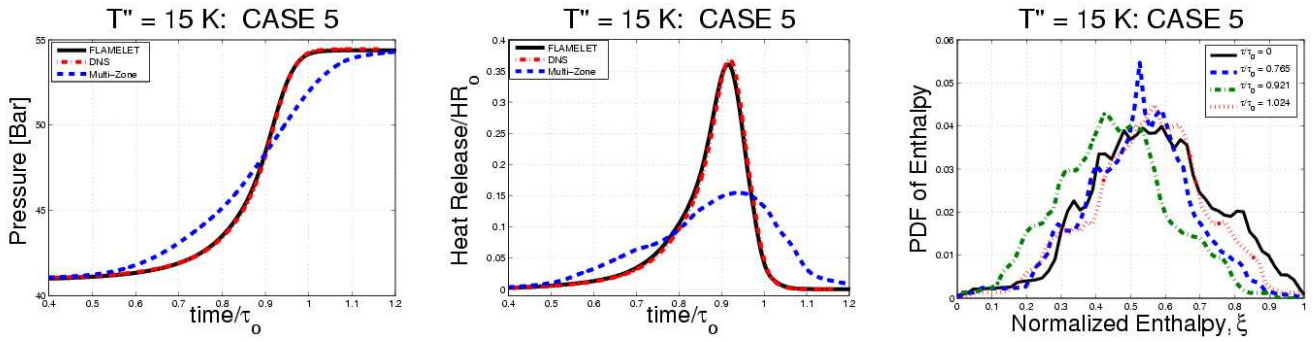

Figure 2: Pressure and normalized heat release versus time and PDF as a function of normalized enthalpy for various times for case 5, T' = 15 K, unity Lewis number.

here defined as,

$$\mathsf{Diff}_{\mathsf{H_2}} = \frac{\rho\chi_\xi}{2}\frac{\partial^2 Y_{H_2}}{\partial\xi^2} \tag{15}$$

$$\mathsf{Chem}_{\mathsf{H_2}} = \rho\dot{\omega}_{H_2}\,. \tag{16}$$

These are plotted at the time of maximum heat release for each of the four cases. As can be seen in these four plots, as the level of enthalpy inhomogeneity increases, the relative importance of the diffusion term increases. For case 1, ($T' = 3.75\,\mathrm{K}$), the diffusion term is negligible compared to the chemistry term. This observation agrees with the DNS analysis by Hawkes et al. [9], where this case was shown to be associated with volumetric combustion. The relative magnitude of the diffusion term for case 4 ($T' = 30\,\mathrm{K}$) is on the order of the chemistry term, which also agrees with the observation in Ref. [9] that this case is largely comprised of deflagration-type burning. Case 2 appears to be mostly chemistry dominated, while case 3 is composed of a mixture of the two combustion modes where diffusion is non-negligible. As observed in the top two rows of this figure, the pressure and heat release rates predicted by the flamelet model are in good agreement with combustion modes ranging from volumetric combustion, mixed modes, and deflagration-type combustion.

Since the flamelet model does not include differential diffusion effects, a fifth DNS case (case 5) with the same conditions as case 3 ($T' = 15K$) but with unity Lewis number was also investigated. The influence of Lewis number on the scalar dissipation rate for species mass fraction, i, scales as $\chi_i \sim D/Le_i + D_{\mathrm{turb}}$. For high Reynolds number flows the turbulent diffusivity is much larger than the molecular diffusivity, $D_{\mathrm{turb}} \gg D$, and therefore turbulent diffusion is dominant and Lewis number effects are not of leading order. The DNS in this study does not have a sufficiently large Reynolds number for this to be the case. However, many applications of this model such as internal combustion engine simulations do have sufficiently large Reynolds numbers for non-unity Lewis number effects to become unimportant. For this reason, case 5 could be thought of, not as a simplification of the physics, but rather a modification that more closely represents higher Reynolds number flows.

The flamelet model and DNS pressure plots (left plot), heat release rate (middle plot), and PDF of enthalpy (right plot) for case 5 are plotted in Fig. 2. In order to compare the flamelet model to a standard type model used in HCCI simulations, results of a multi-zone model from Hawkes et al. [9] are also plotted for the pressure and heat release rate in this figure. The pressure plot shows very good agreement between the DNS and flamelet model, while the multi-zone model predicts a much slower rise in the pressure. It is not too surprising, given that theÊmulti-zone model was not intended toÊperform well in theÊpresence of significantÊdeflagrative burning. But the comparison demonstrates that the multi-zone model is not applicable in situations where diffusion controlled burning occurs. The DNS and flamelet model heat release rates for case 5 are also in very good agreement. Hawkes et al. [9] showed that in case 3 (case 5, but with differential diffusion effects) the reacting front in different regions of the flow exhibited varying levels of ignition-front and deflagration-type burning. For this reason, it is interesting that one flamelet with the mean enthalpy dissipation rate is capable of producing this level of agreement with the heat release rate of the DNS.

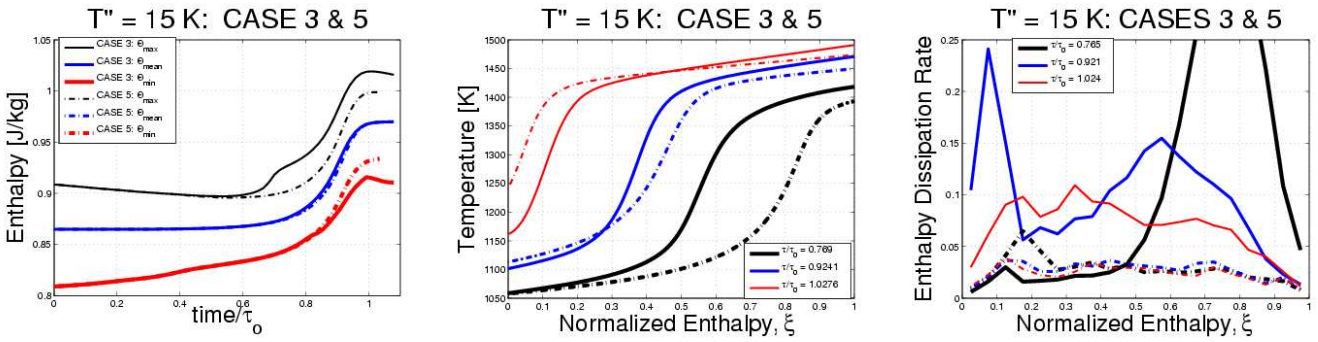

Figure 3: Comparison of cases 3 and 5: left plot: maximum, mean, and minimum enthalpy as a function of time, middle plot: evolution of temperature as a function of normalized enthalpy, right plot: evolution of enthalpy dissipation rate as a function of normalized enthalpy .

Finally, the PDF of enthalpy for case 5 (Fig. 2), similar to cases 2, 3, and 4, shifts toward lower enthalpies during ignition due to the different densities of burnt regions compared to unburnt regions as previously described. Compared to the PDF of enthalpy for case 3 plotted in Fig. 1, however, the PDF shows less shifting toward lower enthalpies because of the absence of differential diffusion effects previously described.

Continuing with the comparison of the differential diffusion case 3 and the unity-Lewis number case 5, the left plot of Fig. 3 shows the maximum, mean, and minimum enthalpies ($\Theta_{\max}$, Θ_{mean}, and $\Theta_{\min}$) of cases 3 (solid lines) and 5 (dashed lines) as a function of time. The influence of hydrogen differentially diffusing to higher enthalpies and thereby increasing the maximum enthalpy for case 3 is observed in this plot by the increase of the maximum enthalpy for case 3 relative to case 5 at a normalized time of 0.7. The effect this has can be seen by comparing the plots of the PDFs of cases 3 and 5 (Figs. 1 & 2). The PDF of enthalpy for case 3 experiences a sharp decrease in value for $0.6 < \xi$ between $\tau/\tau_o = 0.614$ and $\tau/\tau_o = 0.769$. A similar decrease is not observed in the PDF for case 5. The minimum enthalpy for case 3 experiences a departure from case 5 values toward lower enthalpies (left plot, Fig. 3), while the mean enthalpies are relatively unaffected by differential diffusion effects. Temperature as a function of normalized enthalpy, ξ, for cases 3 (solid lines) and 5 (dashed lines) is plotted in the middle plot of Fig. 3 at three times. As can be seen from this plot, the general behavior of combustion for these cases is that regions at higher enthalpies ignite first, followed by a front propagation toward lower enthalpies. The temperature of the burnt gas at $\xi = 1$ for the differential diffusion case is higher than the unity Lewis number case.

Finally, the right plot of Fig. 3 shows the enthalpy dissipation rate, χ_ξ, as a function of normalized enthalpy, ξ, at three different times for these two cases. The enthalpy dissipation rate for the differential diffusion case is much larger than that for the unity Lewis number case. This larger dissipation rate for case 3 accounts for the front advancing faster than case 5 in the middle plot of this figure. Clearly, differential diffusion significantly affects combustion. Considering that the pressure and heat release rates for case 5 are in very good agreement with the DNS results, differential diffusion effects are largely responsible for the discrepancies between the flamelet model results for cases 1, 2, 3, and 4.

CONCLUSION

An enthalpy-based flamelet model for auto-ignition of mixtures with initial temperature fluctuations was presented and applied to five DNS cases with varying levels of thermal inhomogeneity. These cases covered a range of combustion modes from mostly volumetric combustion or ignition fronts to mostly deflagration-type combustion. In the mostly volumetric combustion case, $T' = 3.75\,\text{K}$, the chemical source term was dominant over the diffusion term in the flamelet equation for hydrogen. For the mostly deflagration case, $T' = 30\,\text{K}$, these terms were of the same order. The baseline case, $T' = 15\,\text{K}$, consisted of a mixed mode of both ignition-fronts and deflagrations, where the diffusion term was smaller than the chemical source term, yet exclusion of this term, as is common in multi-zone models, led to greatly

underpredicted maximum heat release rates. The flamelet model showed good agreement with DNS pressure traces and heat release rates for all five cases. This model is capable of capturing the physics associated with both ignition-fronts and deflagrations. Some discrepancy between the flamelet model and the DNS data was observed for the four cases where the DNS included differential diffusion effects. Differential diffusion skewed the PDF toward lower enthalpies, increased the enthalpy dissipation rate, and decreased the effective equivalence ratio of the front. The DNS case with unity Lewis number was absent of any of these differential diffusion effects and was in near perfect agreement with the DNS. At larger Reynolds numbers the non-unity Lewis number effects are not as significant and, therefore, this model is expected to perform well.

ACKNOWLEDGMENTS

This work has been funded in part by Robert Bosch Corporation's Research and Technology Center in Palo Alto, California. The authors would like to thank the RTC Flameless Combustion group: Dr. Aleksandar Kojić, Dr. Jasim Ahmed, and Dr. Sungbae Park for helpful discussions and comments.

Sandia National Laboratories (SNL) is a multiprogram laboratory operated by Sandia Corporation, a Lockheed Martin Company, for the United States Department of Energy under contract DE-AC04-94-AL85000. The work at SNL was supported by the Division of Chemical Sciences, Geosciences and Biosciences, the Office of Basic Energy Sciences, the U.S. Department of Energy. Calculations were performed at SNL and at the National Energy Research Scientific Computing Center, which is supported by the Office of Science of the U.S. Department of Energy under Contract No. DE-AC03-76SF00098. The High Performance Computing and Networking Department at SNL provided access to a 256 processor Infiniband testbed. The authors acknowledge fruitful discussions with Drs. John Hewson, John Dec and Magnus Sjöberg.

APPENDIX

In order to simplify the numeric solution of these equations, the enthalpy field is normalized. The normalization uses variables, $\Theta_{\min}$ and $\Theta_{\max}$, that represent the minimum and maximum enthalpies in the system. They are defined as

$$\Theta_{\min}(\tau) = H_{\min,\mathrm{o}} + \int_{\tau_o}^{\tau} \left(\frac{1}{\rho_{\min}} \frac{\partial p}{\partial t} + \dot{h}_{\min,\mathrm{dif}} \right) dt \tag{17}$$

$$\Theta_{\max}(\tau) = H_{\max,\mathrm{o}} + \int_{\tau_o}^{\tau} \left(\frac{1}{\rho_{\max}} \frac{\partial p}{\partial t} + \dot{h}_{\max,\mathrm{dif}} \right) dt \tag{18}$$

where volumetric heat losses, $q_{\Delta h}$, have been neglected, and $\dot{h}_{\min,\mathrm{dif}}$ and $\dot{h}_{\max,\mathrm{dif}}$ are the temporal change in the minimum and maximum enthalpies caused by diffusion. This term can be thought of as the sum of the effects of wall heat transfer and mixing and is given by

$$\dot{h}_{\mathrm{dif}} = \frac{1}{\rho} \frac{\partial}{\partial x_j} \left(\rho D \frac{\partial H}{\partial x_j} \right) = \dot{h}_{\mathrm{wall}} + \dot{h}_{\mathrm{mix}} \,. \tag{19}$$

The enthalpy field can now be normalized by the maximum and minimum enthalpies.

$$\xi = \frac{H - \Theta_{\min}(\tau)}{\Theta_{\max}(\tau) - \Theta_{\min}(\tau)} = \frac{H - \Theta_{\min}(\tau)}{\Delta\Theta(\tau)} \tag{20}$$

Now a coordinate transformation is performed to transform the flamelet equations from H and τ space into ξ and $\tau^\star$ space. The transformation rules are as follows,

$$\frac{\partial}{\partial \tau} = \frac{\partial \tau^\star}{\partial \tau} \frac{\partial}{\partial \tau^\star} + \frac{\partial \xi}{\partial \tau} \frac{\partial}{\partial \xi} = \frac{\partial}{\partial \tau^\star} + \frac{\partial \xi}{\partial \tau} \frac{\partial}{\partial \xi} \tag{21}$$

$$\frac{\partial}{\partial H} = \frac{\partial \tau^\star}{\partial H} \frac{\partial}{\partial \tau^\star} + \frac{\partial \xi}{\partial H} \frac{\partial}{\partial \xi} = \frac{\partial \xi}{\partial H} \frac{\partial}{\partial \xi} \tag{22}$$

Differentiating Eq.(20) with respect to H and τ gives,

$$\begin{aligned}\frac{\partial \xi}{\partial \tau} &= \frac{1}{\Delta\Theta(\tau)}\left(-\frac{\partial \Theta_{\min}(\tau)}{\partial \tau} - \xi\frac{\partial \Delta\Theta(\tau)}{\partial \tau}\right) \\ &= -\frac{1-\xi}{\Delta\Theta(\tau)}\left(\frac{1}{\rho_{\min}}\frac{\partial p}{\partial t} + \dot{h}_{\min,\mathrm{dif}}\right) - \frac{\xi}{\Delta\Theta(\tau)}\left(\frac{1}{\rho_{\max}}\frac{\partial p}{\partial t} + \dot{h}_{\max,\mathrm{dif}}\right) \qquad (23)\\ \frac{\partial \xi}{\partial H} &= \frac{1}{\Delta\Theta(\tau)} \qquad (24)\end{aligned}$$

Defining new variables λ, λ_0 and λ_1 as

$$\begin{aligned}\lambda(\xi,\tau^\star) &= \frac{1}{\Delta\Theta(\tau^\star)}\left(\frac{1}{\rho(\xi,\tau^\star)}\frac{\partial p(\tau^\star)}{\partial t}\right) \qquad (25)\\ \lambda_0(\tau^\star) &= \frac{1}{\Delta\Theta(\tau^\star)}\left(\frac{1}{\rho_{\min}(\tau^\star)}\frac{\partial p(\tau^\star)}{\partial t} + \dot{h}_{\min,\mathrm{dif}}(\tau^\star)\right) \qquad (26)\\ \lambda_1(\tau^\star) &= \frac{1}{\Delta\Theta(\tau^\star)}\left(\rho_{\max}(\tau^\star)\frac{\partial p(\tau^\star)}{\partial t} + \dot{h}_{\max,\mathrm{dif}}(\tau^\star)\right) \qquad (27)\end{aligned}$$

Substituting Eqs.(23)-(27) into Eqs.(21)-(22) give the coordinate transformations in final form.

$$\begin{aligned}\frac{\partial}{\partial \tau} &= \frac{\partial}{\partial \tau^\star} - \Big((1-\xi)\cdot\lambda_0(\tau^\star) + \xi\cdot\lambda_1(\tau^\star)\Big)\frac{\partial}{\partial \xi} \qquad (28)\\ \frac{\partial}{\partial H} &= \frac{1}{\Delta\Theta(\tau^\star)}\frac{\partial}{\partial \xi} \qquad (29)\end{aligned}$$

In order to simplify this transformation a new variable, which represents a convective velocity in ξ-space, is introduced as

$$v_\xi = \Big(\lambda - (1-\xi)\cdot\lambda_0 - \xi\cdot\lambda_1\Big). \qquad (30)$$

Applying the transformation rules in Eqs.(28) & (29) to the enthalpy space flamelet equations given by Eq.(7) results in the normalized enthalpy-based flamelet equations in final form as given by Eqs.(9) & (10).

References

[1] Christensen, M., et al., *The effect of in-cylinder flow and turbulence on HCCI operation.* SAE Technical Paper, No. 2002-01-2864, 2002.

[2] Epping, K., Aceves, S., Bechtold, R., Dec, J., SAE Paper 2002-01-1923, 2002.

[3] Dec, J., *A computational study of the effect of low fuel loading and EGR on heat release rates and combustion limits in HCCI engines.* SAE Paper 2002-01-1309, 2002.

[4] Aceves, S.M., Flowers, D.L., Westbrook, C.K., Smith, J.R., Pritz, W.J., Dibble, R., Christensen, M., Johansson, B., SAE Paper 2000-01-0327, 2000.

[5] Aceves, S.M., Flowers, D.L., Martinez-Frias, J., Smith, J.R., Westbrook, C.K., Pritz, W.J., Dibble, R., Wright, J.F., Akinyemi, W.C., Hessel, R.P., SAE Paper 2001-01-1027, 2001.

[6] Aceves, S.M., Flowers, D.L., Martinez-Frias, J., Dibble, R., Christensen, M., Johansson, B., Hessel, R.P., SAE Paper 2002-01-2869, 2002.

[7] Kong, S.C. and Reitz, R.D., *Application of detailed chemistry and CFD for prediction direct injection HCCI engine combustion and emissions.* Proc. Combust. Inst., 29, 663-669. 2002

[8] Cook, D.J., Pepiot, P., and Pitsch, H., The Proceedings of The 4th Joint Meeting of U.S. Sections of The Combust. Inst., 2005.

[9] Hawkes, E.R., Sankaran, R., Chen, J.H., and Im, H.G., The Proceedings of The 4th Joint Meeting of U.S. Sections of The Combust. Inst., 2005.

[10] Peters, N., *Turbulent Combustion*, pp. 30-169, Cambridge University Press, 2000.

[11] Mueller, M.A., Kim, T.J., Yetter, R.A., Dryer, F.L, Intl. J. Chem. Kinetics, 31, 113, 1999.